Landau-Darrieus instability and the fractal dimension of flame fronts

Sergei Iv. Blinnikov and Pavel V. Sasorov
Institute of Theoretical and Experimental Physics, B. Cheremushkinskaya 25, Moscow 117259, Russia
(Received 17 April 1995)

Nonlinear dynamics of a slow laminar flame front subject to the Landau-Darrieus instability is investigated by means of numerical simulations of the Frankel equation, when the expansion degree $\gamma=(\rho_u-\rho_b)/\rho_u$ is small (here ρ_u and ρ_b are the densities of the unburned and burned ''gases,'' respectively). Only burning in two-dimensional space is considered in our simulations. The observed acceleration of a front wrinkled by the instability can be ascribed to the development of a fractal structure along the front surface with typical spatial scales being between the maximum and the minimum truly unstable wavelengths. It is found that the fractal excess $\Delta D=D-1$ decreases rapidly with decreasing of γ, to a first approximation as $\Delta D=D_0\gamma^2$, where D is the fractal dimension of the front. Our rough estimation of D_0 gives $D_0\approx 0.3$. The low accuracy of the D_0 estimation is caused by certain peculiarities of the Frankel equation that lead to extreme difficulties of its simulation even with the aid of supercomputers when $\gamma\lesssim 0.3-0.4$. It is shown, however, that D_0 can be calculated also from the statistical properties of the Sivashinsky equation, which is easier to simulate, though the fractal excess for the Sivashinsky equation itself is equal to 0 (in a certain sense). The other important result of our simulations is that the front self-intersections play an extremely weak role when γ is small. [S1063-651X(96)02605-0]

PACS number(s): 47.11.+j, 47.20.−k, 47.53.+n, 82.40.Py

I. INTRODUCTION

In large volumes of premixed fuel, the combustion process, or flame, can propagate either in the form of a supersonic detonation wave or in the form of a relatively slow deflagration wave [1]. In the first case, the unburned fuel is ignited by a shock front propagating slightly ahead of the burning zone itself. In the second case, ignition of new fuel portions is governed by heat and active reactant transport, i.e., by thermal conduction and diffusion. In the latter case, the flame propagation velocity can be much less than the sound velocity. So the gas pressure is almost uniform and both burned and unburned gases can be treated as almost incompressible fluids outside the flame zone.

The subject of this paper is the slow deflagration regime of the flame propagation. It is well known [1–5] that large portions of a slow planar flame front are unstable with respect to the large-scale bending. This universal instability, which is called the Landau-Darrieus (LD) instability, does not depend, for sufficiently long wavelengths, on complex physical and chemical processes that take place in the burning zone and in the presence of various short-wavelength instabilities caused by these processes (see, for example, Ref. [5]). Development of the LD instability depends only on the sign of $\Delta\rho=\rho_u-\rho_b$, where ρ_u and ρ_b are densities of the unburned and burned ''gases,'' respectively. The LD instability of planar flame fronts with respect to large-scale bending takes place if and only if $\Delta\rho>0$. We suppose below that there are no other instabilities of the slowly moving flame fronts except for the LD instability.

As explained in the original paper by Landau [2], the LD instability leads to wrinkling or roughening of the front surface, i.e., to increasing its area with respect to the smooth front, and consequently to acceleration of the front propagation. In extreme cases, the LD instability can lead to a transition from the regime of slow flame propagation to the regime of detonation. These features of the LD instability play an important role in many physical phenomena such as usual chemical burning of gases in terrestrial conditions, explosive boiling of liquids [6], dynamics of thermally bistable gas [7], and thermonuclear burning of the stellar core in the progress of supernova explosions of type Ia [8,9].

It is necessary to emphasize here that usually there is a vast range of spatial scales unstable with respect to the LD instability in the astrophysical objects such as supernova explosions mentioned above. A very rough estimation of the ratio between the maximum and the minimum scales of front wrinkles can be given by the ratio of the radius of the considered system to a laminar flame thickness. This ratio can reach $10^{10}-10^{13}$ for the case of supernova explosions, which excludes any possibility of direct numerical simulations of the LD instability effects on such conditions and requires an analytical approach to describe the propagation of a wrinkled front.

A proper heuristic idea for this case is the concept of fractal surfaces and appropriate fractal dimensions. The idea of applying fractals to the flame physics was put forth in Refs. [10–12]. By a fractal surface we mean an irregular surface whose statistical properties change self-similarly with a change of the considered scale. A scale range in which this similarity holds, which will be called the similarity range, is assumed to be sufficiently wide in logarithmic scale. Let $\lambda_{\min}$ and $\lambda_{\max}$ be, respectively, the minimum and the maximum lengths belonging to this similarity range. The fractal dimension of the front surface is a number D, which obeys the inequality $2\leqslant D\leqslant 3$, such that the total area of the typical portion of this surface with a diameter L is proportional to L^D, when L varies in the range $\lambda_{\min}\leqslant L\leqslant\lambda_{\max}$.

If the front structure behaves like a usual smooth surface with $D=2$ outside the similarity range, then the area of the front surface, corresponding to the flame front developing from a small igniting region, can be estimated as

$$S \approx 4\pi R^2 \left(\frac{\lambda_{\max}}{\lambda_{\min}} \right)^{D-2}, \tag{1}$$

where R is the radius of a sphere whose volume is equal to the volume occupied by the burned gas. Since the mass flux across the flame front depends only weakly on the front curvature, when the curvature radius belongs to the similarity range, the mean velocity of the front relative to the burned gas

$$u = \frac{dR}{dt} \tag{2}$$

should be renormalized as

$$u = u_0 \left(\frac{\lambda_{\max}}{\lambda_{\min}} \right)^{D-2}, \tag{3}$$

where u_0 is the propagation velocity of the planar laminar front measured relative to the burned gas.

The features of the front surface should depend on the expansion degree

$$\gamma = \frac{\rho_u - \rho_b}{\rho_u} \tag{4}$$

and on R. If a fractal surface is a good enough approximation to the front properties, then $\lambda_{\min}$, $\lambda_{\max}$, and D should tend, after sufficiently long temporal evolution of the propagating flame, i.e., for sufficiently large R, to

$$\lambda_{\min} = l_{\min}(\gamma), \tag{5}$$

$$\lambda_{\max} = \alpha_{\max}(\gamma) R, \tag{6}$$

$$D = D(\gamma). \tag{7}$$

If we define $\lambda_{\min}$ as a mean distance between adjacent local maxima of absolute values of the front principal curvatures multiplied by 2, then Eqs. (1) and (3) define $D(\gamma)$ and $\alpha_{\max}$ in the limit of $R \to \infty$. Determination of $\lambda_{\min}$, $\lambda_{\max}$, and D, when $R \to \infty$, i.e., of $l_{\min}(\gamma)$, $\alpha_{\max}(\gamma)$, and $D(\gamma)$, is the main objective of the theory of moving wrinkled flames.

It is impossible to do this in one step. So we shall investigate here only a particular case when the expansion degree γ tends to zero. A solution of this problem can help to approximate the flame propagation in some applications of this theory. The most striking example is the supernova explosions of type Ia mentioned above, which requires evidently the development of the theory and where typical values of γ belong to the range of 0.1–0.5 [12,15], with the major portion of the flame propagation region corresponding to the γ range of 0.2–0.3. Thus the limit of $\gamma \to 0$, which will be considered in this paper, can be a satisfactory zeroth-order approximation. Definitions (1)–(3) are widely used in the literature. See, for example, Refs. [13,14].

We recall here some methods used for the description of the thin front dynamics. By the way, there are many similarities between the thermally bistable gas dynamics and the slow conductive flame front propagation. The most general equations neglecting any reactions and diffusion outside a very thin front were quoted in a paper [7] devoted to the thermally bistable gas dynamics. The relevant set of equations is called there a system of ''superreduced equations.'' The only consequence of the finite front thickness was the existence there of the so-called Markstein diffusivity D_M [16], which describes the tendency of a flame to smooth out the roughness of its front at small spatial scales. A method for the calculation of Markstein diffusivity, which is suitable in some cases just for thermally bistable gases, was presented in Ref. [7]. Other methods that are applicable for investigations of many local properties of the flame fronts and are more appropriate for chemical reactions, obeying the Arrhenius law with the high value of the so-called Zeldovich number, were published earlier [17,18]. The case of the moderate Zeldovich number is considered in Ref. [19].

If the expansion degree γ is sufficiently small so that the flow of matter both behind and ahead of the front can be approximated by the potential velocity field, then the equations of matter motion outside the front can be solved in general and the whole set of front dynamics equations can be reduced to a single equation *on* the front surface. This was done by Frankel [20]. The well known Sivashinsky equation [21,22], which is well known in investigations of wrinkled surfaces and moving fronts of different nature, is derived by Frankel [20] from his equation assuming a small slope of the disturbed front with respect to the reference plane or sphere. The Frankel as well as the Sivashinsky equations will be widely used in the present work.

There is some experimental evidence [11] that the fractal dimension of the slow flame front could be equal to 7/3. This seems to have been confirmed recently by the relevant simulations of the Sivashinsky equation [23]. These results, if they have a wide field of applicability, could lead to drastic consequences in the theory of supernova explosions: due to Eq. (3) the slow flame propagation would virtually be impossible for $D=7/3$, given the enormous similarity range in presupernova white dwarfs. The results of Refs. [11,23] as well as of Refs. [12,15] have encouraged us to carry out this work where we focus our attention more carefully to flame fronts wrinkled by the LD instability under the condition of low expansion degree γ.

Our main results are as follows.

(i) The bending degree of the flame front under the action of the fully developed LD instability depends strongly on the expansion degree γ, as seen from numerical simulations of the Frankel equation.

(ii) Decreasing γ leads to very weak wrinkling of the flame and to a weak role of the front ''self-intersections.''

(iii) The fractal excess of the wrinkled front surface can be approximated by the formula

$$\Delta D = D_0 \gamma^2, \tag{8}$$

with its functional form proven analytically and verified numerically. Our numerical simulations give $D_0 \approx 0.3$ for the two-dimensional case when the front is actually a curve.

(iv) The fractal excess of the Sivashinsky equation determined by using Eq. (3) is rigorously equal to 0.

(v) Nevertheless, the simplest way to calculate D_0 in Eq. (8) is to calculate a two-point correlation function for the Sivashinsky equation. This is a consequence of unexpected difficulties of the Frankel equation simulation even with the aid of supercomputers.

The body of this paper is organized as follows. Section II is devoted to the derivation of the Frankel and the Sivashinsky equations and to their main properties, which are necessary to our investigation. Methods of simulations of the Frankel equation are considered in Sec. III. The main general results of these simulations are presented in Sec. IV. Some properties of fractal lines with low fractal dimensions are considered in Sec. V, using the generalized Koch line as an example. A relationship between the two-point correlation function for the Sivashinsky equation and the fractal dimension of the front governed by the Frankel equation is investigated in Sec. VI. This relationship helps us to prove Eq. (8) for these fronts, when $\gamma \to 0$. Results of the Frankel equation simulations, which are particularly aimed at the fractal dimension determination, are presented in Sec. VII. They allow us to evaluate the constant D_0 in Eq. (8). It should be emphasized that our results of the simulations including the value of D_0 concern only the two-dimensional case when the front is in fact a curve. Nevertheless, our main analytic results including the analytic form of Eq. (8) can be generalized also to the three-dimensional case. This is explained in Sec. VIII. Our general results, their main consequences, and further problems are discussed in Sec. IX.

II. THE FRANKEL AND SIVASHINSKY EQUATIONS

Suppose that the flame front is sufficiently thin with respect to other scales and its velocity is sufficiently low with respect to the sound speed, whereas no other forces with the exception of pressure gradients are applied to matter. Then the flow both ahead and behind the flame front can be treated as incompressible, so that the vorticity $\vec{\omega} = \mathrm{curl}\vec{v}$ is governed by the so-called freezing-in equation

$$\frac{\partial \vec{\omega}}{\partial t} = \mathrm{curl}(\vec{v} \times \vec{\omega}), \tag{9}$$

where $\vec{v}$ is the fluid velocity. If initially there was no macroscopic motion before the flame ignition localized in a small singly connected region, then $\vec{\omega} = \vec{0}$ ahead of the flame front, in accordance with Eq. (9). According to Eq. (9), the vorticity can be generated only near the front where the density is not uniform and it is carried away downstream (relative to the front). However, if the front preserves its spherical or planar shape, then the flow is obviously potential (i.e., $\vec{\omega} = \vec{0}$) even behind the front.

To evaluate a role of the vortical component $\vec{v}_v$ of the velocity field in comparison with the nonuniform part of the potential component $\vec{v}_{\mathrm{NP}}$ in the vicinity of the front it is possible to use the linear theory of the LD instability (see Ref. [3] for details) which is valid for this purpose in the case when $h \ll \lambda$, where h is the deviation of the front position from its unperturbed position and λ is a typical wavelength of the front disturbances. It is necessary to note here that $h/\lambda \sim \gamma \ll 1$ even for the fully developed LD instability when $\gamma \to 0$ (see Sec. VI below). Thus we have

$$|\vec{v}_v|/|\vec{v}_{\mathrm{NP}}| \sim \gamma, \tag{10}$$

with $|\vec{v}_{\mathrm{NP}}|$ being of the order of $\gamma u_0 h/\lambda$. It is seen that the vortical component of the field velocity can be neglected in the first approximation under the conditions $\gamma \ll 1$ and $\lambda \gg l_D$, where l_D is the thickness of the diffusion zone of the flame front [24].

We proceed now to a brief derivation of the Frankel equation governing the slow flame dynamics for the case where $\gamma \ll 1$ and $\lambda \gg l_D$. We consider here only the two-dimensional case, when the front is actually a curve.

The velocity components, tangential with respect to the front, must be continuous in this approximation [7,18], hence the entire velocity field can be assumed to be potential, with the velocity potential being a harmonic function outside the front thermal zone due to incompressibility of matter there. A reference frame can be chosen in such a way that the velocity of the unburned matter tends to zero at infinity. The mass conservation law determines the jump of the normal velocity component across the front, so that the velocity can be expressed as the gradient of a single layer potential with surface density determined by the mass flux across the front (see Ref. [20]). Assuming the flame front to be a finite closed curve ignited in a small portion of initially motionless unburned matter, we may write the following Frankel-like equation for the normal velocity of the front propagation (see Ref. [20]):

$$U(\vec{x},t) = \frac{J(\vec{x},t)}{\rho_b} - \frac{\gamma}{2\rho_b}\left(J(\vec{x},t) - \frac{1}{\pi} \oint_{\Sigma(t)} J(\vec{\xi},t) \frac{(\vec{x}-\vec{\xi})\cdot\vec{n}(\vec{x},t)}{|\vec{x}-\vec{\xi}|^2} dl_\xi \right). \tag{11}$$

Here $\Sigma(t)$ is the moving curve line corresponding to the flame front; dl_ξ is a differential of its length; $\vec{n}$ at fixed t is a smooth unit vector field that is normal to the front line Σ pointing towards the unburned matter; $J(\vec{x},t)$ is the mass flux across the front, which depends in general on the position $\vec{x}$ of a point on the curve Σ; and the positive sign of U is chosen to correspond to the direction of $\vec{n}$. Points $\vec{x}$ and $\vec{\xi}$ in Eq. (11) belong to $\Sigma(t)$. This conforms to the fact that $U(\vec{x})$ and $J(\vec{x})$ are defined for $\vec{x} \in \Sigma(t)$ only. The motion of Σ can be described by the motion of points belonging to it, so that

$$\frac{d\vec{x}(t)}{dt} = \vec{n}(\vec{x},t)U(\vec{x},t) \quad \text{for} \quad \vec{x}(t) \in \Sigma(t). \tag{12}$$

The mass flux J_0 across a planar front, which is actually a straight line in this case, is a physical constant for a given fuel at fixed (by assumption) external pressure. If the front is curved only slightly, then its curvature can be treated perturbatively, assuming that the ratio of the front diffusion thick-

ness to its typical curvature radius is a necessary small parameter. As mentioned in the Introduction, the relevant theory is further elaborated after the pioneering work by Markstein [16]. See Refs. [17–19,7,3–5,14]. Thus we can write

$$J(\vec{x},t)=J_0-\rho_b D_M \mathscr{K}(\vec{x},t), \tag{13}$$

where $\mathscr{K}(\vec{x},t)$ is a curvature of the curve $\Sigma(t)$ at the point $\vec{x}\in\Sigma(t)$, with $\mathscr{K}$ being positive when the front is convex towards the unburned matter; D_M is the Markstein diffusion coefficient [16]. The second term on the right-hand side of Eq. (13) is assumed to be much less than the first one. D_M is usually positive when the thermal conduction is a more efficient process than the molecular diffusion of reactants (see Refs. [17,18]). We suppose below that $D_M>0$. Instead of D_M, the Markstein length $l_M=\rho_b D_M/J_0$ is frequently used. As a rule, l_M is a little larger than the typical front thickness l_D. The curvature $\mathscr{K}$ can be expressed in terms of the derivatives of $\vec{n}$: $\mathscr{K}=(\operatorname{div}\vec{n})|_\Sigma$.

It will be seen from our results that a maximum absolute value of the curvature of the flame front wrinkled by the LD instability is of the order of γ^3/l_M, so that Eq. (13) is applicable here. Besides that, since the correction to $J(\vec{x},t)$, caused by the front curvature, is of order γ^3, this correction should be taken into account only in the first term on the right-hand side of Eq. (11). One should remember that these terms can be considered as only two first nonzero terms of a series in powers of γ of an ''exact'' expression for U. Let us introduce new units, so that the length is measured in l_M, the time in l_M/u_b, and density in ρ_b, and let us refer to this system as Markstein units. In these units $J_0=D_M=1$ and the reduced dimensionless form of Eq. (11) can be written as

$$U(\vec{x},t)=1-\operatorname{div}\vec{n}(\vec{x},t) - \frac{\gamma}{2}\left(1-\frac{1}{\pi}\oint_{\Sigma(t)}\frac{(\vec{x}-\vec{\xi})\cdot\vec{n}(\vec{x},t)}{|\vec{x}-\vec{\xi}|^2}dl_\xi\right). \tag{14}$$

This is the Frankel equation [20] with the account of the Markstein stabilization of the LD instability at short wavelengths. It contains single dimensionless parameter γ, which should be considered as $\gamma\to 0$. Only this dimensionless form of the equation will be used below.

Let us suppose now that in some Cartesian system of coordinates (x,y) the front Σ can be defined by the equation

$$y=t+h(x,t), \tag{15}$$

with

$$|\partial h/\partial x|\ll 1 \tag{16}$$

and with the region $y>t+h(x,t)$ corresponding to the unburned matter. Then, in a reference frame where the burned matter at $y\to-\infty$ is motionless, the evolution of this surface obeying Eq. (14) can be described, in accordance with Ref. [20], by the equation

$$\frac{\partial h}{\partial t}+\frac{1}{2}\left(\frac{\partial h}{\partial x}\right)^2=\gamma I\{h\}+\frac{\partial^2 h}{\partial x^2}. \tag{17}$$

Here

$$I\{h\}(x)=\frac{1}{4\pi}\int |k|h(\zeta)\exp ik(x-\zeta)dkd\zeta. \tag{18}$$

Equation (17) was formulated by Sivashinsky in Ref. [21]. A more general equation is suggested in Ref. [25].

The dimensionless parameter γ can be eliminated from Eq. (17) if we introduce a scaled function

$$\eta(x,t)=h(x/\gamma,t/\gamma^2) \tag{19}$$

instead of $h(x,t)$ (cf. [26]). Thus the function η obeys the following form of the Sivashinsky equation:

$$\frac{\partial \eta}{\partial t}+\frac{1}{2}\left(\frac{\partial \eta}{\partial x}\right)^2=I\{\eta\}+\frac{\partial^2 \eta}{\partial x^2}. \tag{20}$$

This means that the Sivashinsky equation (20), as well as (17), does not actually contain any dimensionless parameters in contrast to the Frankel equation (14). Equation (20) is invariant with respect to the mapping

$$\eta(x,t)\to\overline{\eta}(x,t)=cx-\frac{1}{2}c^2t+\eta(x-ct,t)+\eta_0 \tag{21}$$

for any constant c and η_0. This property shows, in particular, that there is only a trivial interaction between two disturbances if the ratio of their wavelengths is much greater than unity. The Sivashinsky equation (20) has another important property for solutions with extremely large spatial scales when the last term on the right-hand side of Eq. (20) is negligible. Then the equation

$$\frac{\partial \eta}{\partial t}+\frac{1}{2}\left(\frac{\partial \eta}{\partial x}\right)^2=I\{\eta\} \tag{22}$$

preserves its form under the action of the scaling

$$\eta(x,t)\to\overline{\eta}(x,t)=\mu\,\eta(x/\mu,t/\mu) \tag{23}$$

for each $\mu>0$.

The Frankel equation (14) has a symmetry corresponding to a rotation of the coordinate system by an arbitrary finite angle around its origin and to any displacement of the latter. But the Sivashinsky equation is not rotationally invariant with respect to the rotation of the coordinate system in the ambient space because the condition (16) had been used for its derivation. This condition is not rotationally invariant. Nevertheless, the invariance (21) of the Sivashinsky equation can be considered as a consequence of the rotational symmetry of the Frankel equation.

It is widely admitted that the Sivashinsky equation plays a significant role in many branches of nonlinear physics. For this reason it was investigated in a number of works [26–30]. The elegant analytic method developed in Ref. [29] gives a wide set of exact solutions of Eq. (20); some properties of these solutions will be used below.

The Frankel equation was derived rigorously. That is why we presented above the main steps of its derivation. This cannot be said about the Sivashinsky equation (20). Indeed, the necessary condition (16) for its applicability is easily violated if the ratio $\lambda_{\max}/\lambda_{\min}$ is sufficiently large even for

small γ. Nevertheless, this equation is extremely useful for investigations of the Frankel equation properties, as will be seen in Sec. VI below.

III. NUMERICAL TECHNIQUE FOR FLAME SIMULATION WITH THE FRANKEL EQUATION

For numerical experiments with an initial value problem for the two-dimensional Frankel equation (14) we have used the following discretization. Each piece of the front is represented by a mesh point with coordinates (x_i,y_i), so that the set of the points $\{x_i,y_i\}$ with $i=0,1,2,\ldots,N,N+1$ and $(x_i,y_i)\equiv(x_{i+N},y_{i+N})$ for $i=0,1$ forms an approximation of a closed curve modeling the front. The step of the mesh along the front is defined as

$$s_i=[(x_i-x_{i-1})^2+(y_i-y_{i-1})^2]^{1/2}. \tag{24}$$

An important quantity is then defined

$$\Delta l_i=(s_i+s_{i+1})/2. \tag{25}$$

The quantity Δl_i may be called the mesh point weight since it reflects the contribution of the point to the velocity potential. The total number of points N is variable: it is not allowed to decrease, but it may grow to adapt the peculiarities of the front. The weight Δl_i is kept to be bounded in the range $l_{\min}<\Delta l_i<l_{\max}$ for each $i=1,2,\ldots,N$. When the neighboring mesh points are too close, one of them (with the minimum weight) is deleted, but N is kept fixed, so an additional mesh point appears in the middle of the interval with maximum step s_i. When the neighboring points are too distant, a mesh point is inserted between them, so N is increased. After numerical experiments the values of $l_{\min}=0.2$ and $l_{\max}=10$ in the Markstein units were chosen.

For each point i we use its neighbors $i-1$ and $i+1$ to build a circumference going through these three points. The radius of the circumference R_i gives the curvature of the front at the point i, so that $\mathrm{div}\vec{n}_i=1/R_i$ with the second-order accuracy relative to Δl_i. The direction to the center of the circumference gives, to the same accuracy, the direction of the local normal $\vec{n}_i$.

Now we have for each point a set of N ordinary differential equations (12), where U is taken from the discrete version of the Frankel equation (14). There are two nontrivial moments in this equation: the diffusion term $\mathrm{div}\vec{n}_i$ and the integral over the whole length of the front, which must be computed anew for each point. In an explicit scheme the time step is bounded by the Courant condition, i.e., it must be of $O(\min(\Delta l_i)^2)$. Sometimes this may be too restrictive, so we have developed an implicit numerical code employing a predictor-corrector integrator for obtaining the solutions to Eqs. (12) and (14). It would be too hard to invert the huge Jacobian needed for Newton's iterations, so to find the solution of the equation for the corrector simple iterations were used (the method of a fixed point). The convergence of this algorithm also imposes a restriction on the time step, but not as stiff as the Courant condition. Another advantage of a predictor-corrector scheme is the natural way to control the error by comparing the predicted and corrected values of (x_i,y_i). The scheme is based on the widely tested Gear algorithm [31] with options for implicit Adams and Brayton-Gustavson-Hachtel [32] schemes with an automatic choice of the time step and of the order of the method.

The integral in Eq. (14) is approximated by the formula of rectangles [$\vec{\xi}$ is identified with a point (x_j,y_j) and dl_ξ is just replaced by Δl_j and for each i the sum over $j=1,2,\ldots,N$ is taken with a special treatment of the case $j=i$]. This algorithm costs $O(N^2)$ operations, which is too much when N is of the order of a few thousand. To reduce the cost, it is natural to apply here algorithms employing a hierarchical tree construction for calculating N-body interactions. In our code the integral is computed by the Barnes-Hut method [33] with a vectorizable algorithm analogous to that developed by Hernquist [34] and Makino [35]. This method allows us to perform tree construction and potential evaluation in $O(N\ln N)$ operations. In our implementation of the method the mass of particles is replaced simply by the weights Δl_i of the mesh points. Thus the calculation of the velocity potential is quite similar to force calculations in Refs. [33–35]. The main difference with the cited works is the treatment of the motion of the mesh points or ''particles'': it is necessary to take into account that in our set they are not completely free—the ordering of N points along the front must be preserved at any time step.

The accuracy of potential calculations was tested by comparing the results with analytical formulas for the potential of a circumference segment with constant linear density. The stability of the algorithm was tested by computing the evolution of a quasicircular front with a small initial radius for low values of the density jump γ. For such initial conditions all low-amplitude perturbations actually die out in our numerical simulations as long as the mean radius of the front remains smaller than the critical radius for given γ; cf. Ref. [3].

It is necessary to notice that the front curves governed by Eq. (14) can become self-intersecting. However, a real flame front cannot be self-intersecting. Hence Eq. (14) should be completed by the so-called reconnection rule. The process of reconnection, expected from a physical point of view, is described by Fig. 1.

In actual simulations we avoided complications with the appearance of the multiply connected structure of flames merely removing the mesh points, which tend to produce an intersection of the front. Thus the ''lake'' of unburned matter, shown on the right-hand side of Fig. 1, remains connected by a narrow ''channel'' with the ''ocean'' of the fuel and the lake quickly disappears. This is some violation of the physical picture, but we find that the intersection of distant parts of the front is encountered only for large values of γ, when the validity of the potential approximation does not hold and the Frankel equation does not describe physical flames (see illustrations and discussion in the following sections). Nevertheless, the precautions against the front intersections are implemented in the code: the nontrivial monitoring of the mesh points, which are not neighbors along the front but which approach each other to a dangerous proximity, is done with the aid of vectorizable procedures similar to those described in [34] for the nearest-neighbor searching with the aid of the tree structure built for the potential calculation.

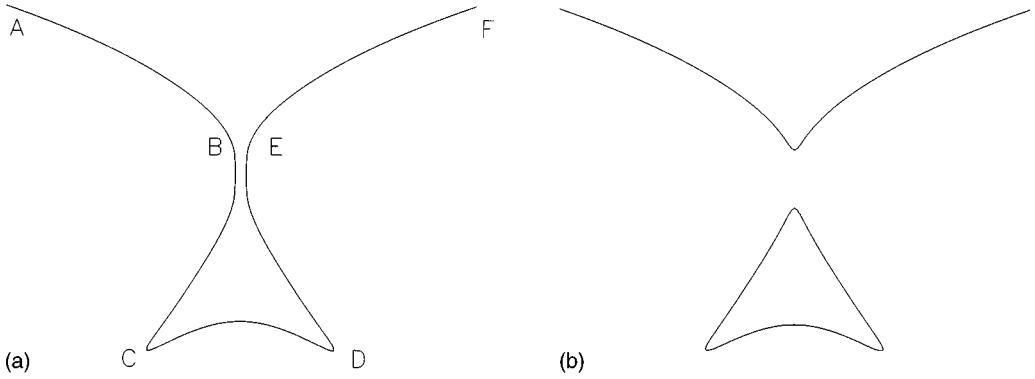

FIG. 1. Process of the front reconnection when the self-intersection can take place. The front patterns for two moments of time are represented. For easier viewing they are separated from each other. The front propagates upward, where the unburned matter is placed.

As is well known, the LD instability leads to the formation of cusps directed to the burned matter [3,21]. In our simulations of the Frankel equation the cusps are smoothed by the Markstein diffusion and by our prescription to remove the points with a low value of Δl. Yet it is not a rare event even for small γ that the neighboring mesh points moving near a cusp tend to produce an intersection of the front. We forbid this by imposing a restriction on the minimum angle at the vertex of a cusp: each mesh point at a vertex having an angle less than the allowed minimum is removed from the mesh. The value of 0.03 rad was chosen for the minimum allowed angle.

IV. PRELIMINARY RESULTS OF THE SIMULATION

In this section we present the results of simulations of the Frankel equation concerning the general properties of this equation. We are interested in the properties of the Frankel equation itself, regardless of the fact that it models flame propagation only at $\gamma \to 0$.

The global features of the front and their temporal evolution for two values of $\gamma = 0.8, 0.4$ as obtained by the Frankel equation simulations described above are presented in Figs. 2 and 3. The initial front shape is a circle with a regular small-amplitude sinusoidal perturbation along the x coordinate. The initial conditions are quickly forgotten in the case of $\gamma = 0.8$, but they persist for a longer time when $\gamma = 0.4$. The front consists of arcs, which are convex towards the unburned matter with sharp cusps near their connections, which are directed towards the burned matter. This agrees with the well known properties of the Sivashinsky equation [21], which are manifested by even its analytic solutions [29].

It can be seen that the front pattern for $\gamma = 0.4$ differs drastically from that for $\gamma = 0.8$. The front is strongly corrugated for $\gamma = 0.8$, but only weakly wrinkled when $\gamma = 0.4$. The pattern structure for $\gamma = 0.4$ is hardly distinguishable. This difference cannot be explained by assuming that the instability has not yet developed for lower γ. In fact, fully developed LD instability in the strongly nonlinear regime takes place at final times for both cases and for all really unstable wavelengths. The growth rate of the instability depends on γ (see Ref. [2]). For small γ it is just proportional to γ. This is reflected particularly in Eq. (17), which repro-

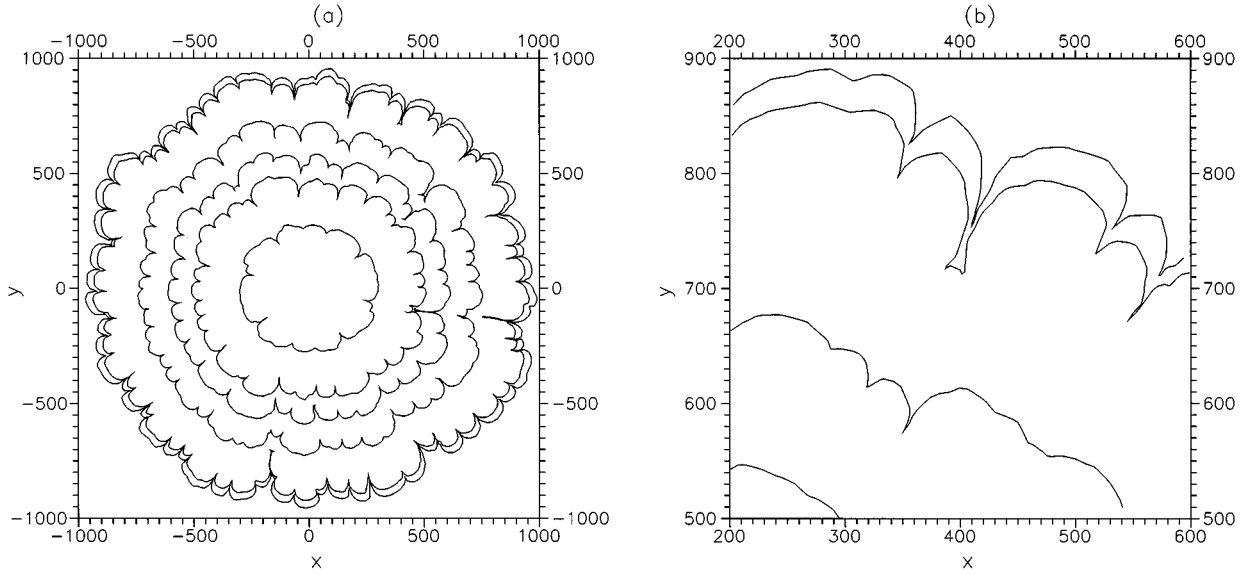

FIG. 2. (a) Front pattern for $\gamma = 0.8$ at different times $t = 158,309,377,467,586,604$. Length and time are measured in Markstein units. The window (b) is a blowup of a portion of the window (a).

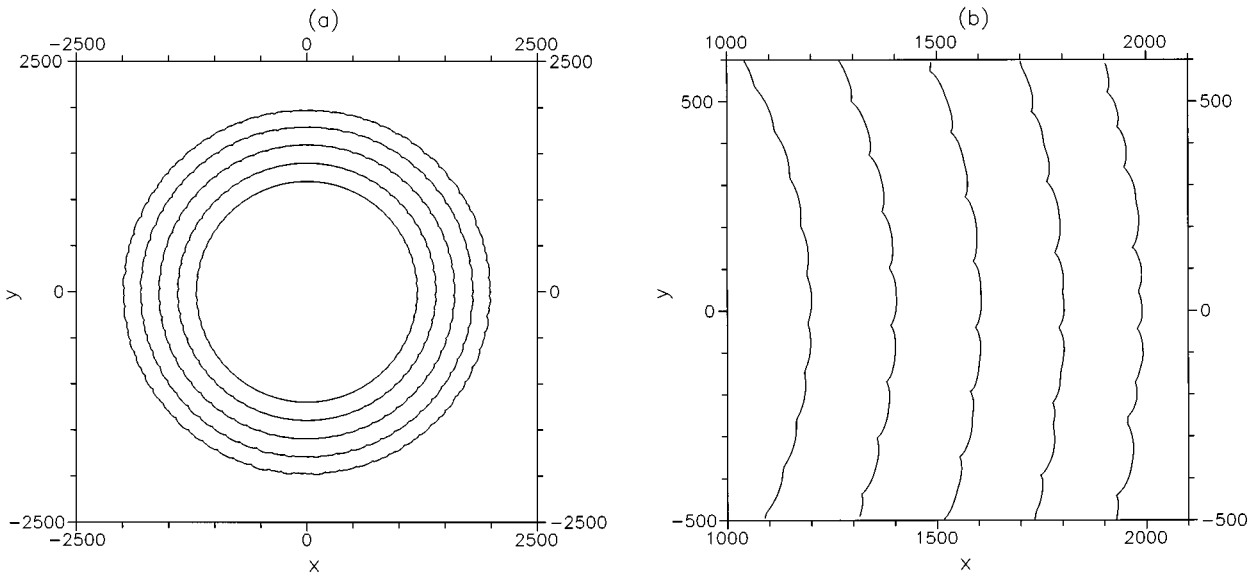

FIG. 3. Front pattern for $\gamma=0.4$ in two different scales for the moments of time $t=197{,}394{,}592{,}785{,}966$.

duces the Landau-Darrieus growth rate for small γ. However, a slower development of the instability for $\gamma=0.4$ is compensated for by a longer time of simulation.

More attentive examination of these pictures reveals that there are two quantitative reasons responsible for the strong difference between the two patterns. First, the unstable wavelengths range for $\gamma=0.4$ is sufficiently narrower than for the $\gamma=0.8$ case. Indeed, the longest unstable wavelength is proportional to γ for a circular flame, whereas the shortest one is inversely proportional to γ. It is a direct consequence of the linear theory (see, for example, Ref. [3]) and is not so interesting from the viewpoint of the nonlinear theory.

Second, the relative degree of nonlinear saturation, i.e., the ratio h/λ, for the $\gamma=0.4$ case is significantly lower than for the $\gamma=0.8$ case. Here h is a deviation of the front position from the nearest reference circle and λ is a typical wavelength of disturbances. This fact is more evident in Fig. 3(b), where a portion of the front is represented with a more appropriate scale factor. It is almost evident that this leads to a smaller fractal dimension of the front for the smaller γ. This issue will be discussed in some detail in the following sections, but it is worth noticing now that the front fractal dimension D seems to fall drastically when γ decreases down to 0.4 or, generally speaking, D seems to depend strongly on γ, decreasing together with γ. If this is so, then it leads to a more important influence on the renormalized flame speed (3) when the ratio $\lambda_{\max}/\lambda_{\min}$ is sufficiently high than changing of this ratio itself.

There are some other conclusions that can be drawn from the analysis of the results presented in Figs. 2 and 3. The longest unstable wavelength is satisfactorily described by the linear theory for a circular front [3]. This theory takes into account stretching of disturbances along the front due to its radial expansion. The shortest wavelength, really unstable for finite amplitudes, is determined by a similar effect, but stretching is caused now by disturbances with longer wavelengths, so it is actually some nonlinear effect that was considered in Refs. [3,21,4]. Our simulations show that the shortest really unstable wavelength, which is actually $\lambda_{\min}$, can be approximated as $(30-40)/\gamma$.

Self-intersections of the front are another phenomenon that can be easily detected in Fig. 2 but is absolutely not seen in Fig. 3. We have never observed self-intersections of distant parts of the front for γ less than 0.5.

V. SOME PROPERTIES OF CURVES WITH LOW ΔD: EXAMPLES

As shown both by preliminary results of the Frankel equation simulation and by a special investigation presented below, the fractal excess $\Delta D=D-1$ of the flame ''surface,'' which is actually a curve for two-dimensional ambient space, is very small for small γ. But fractal lines with a small fractal excess have some important peculiarities. To illustrate them, we consider here the generalized example of a curve introduced first by von Koch in 1906 (see, e.g., Sec. 13.2 in [36]). This example seems to mirror some basic properties of the results of simulations quoted above. An analogy between Koch triads and the shapes of expanding flames in laboratory experiments was noted in [11].

The generalized Koch curve K_θ is determined as a limit of a sequence $\{K_{\theta,n}\}$ $(n=1,2\ldots)$ of curves $K_{\theta,n}$. Each member $K_{\theta,n}$ of this sequence is a broken line, consisting of segments of the same length, and this broken line is constructed from the previous member of the sequence $K_{\theta,n-1}$ by an iterative procedure. Each step of the iteration replaces each line segment, i.e., each link of the broken line $K_{\theta,n-1}$, by the scaled ''basic'' broken line, which is similar to that depicted in Fig. 4. The geometrical characteristics of this basic broken line are defined in Fig. 4(b). The first member of the sequence is a line segment of unit length. It is useful to introduce two other geometrical parameters of the basic broken line, namely, (a) the ratio of the length of the segments to the diameter of the basic line

$$f=\frac{1}{2(1+\sqrt{1-\theta^2})} \tag{26}$$

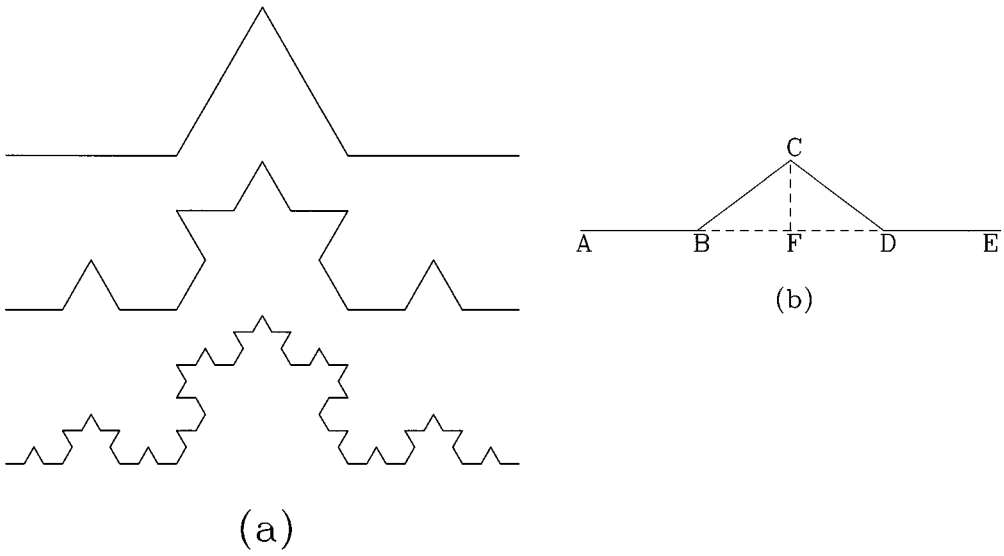

FIG. 4. (a) Three initial steps of the Koch example. (b) The broken line $ABCDE$, which replaces the upper broken line in (a) in the construction of a generalized Koch curve. $|AB|=|BC|=|CD|=|DE|\equiv l$. $h\equiv|CF|$, $\theta=h/l$, and $f\equiv l/|AE|$ are the parameters used in the text.

and (b) the ratio of the total length of the basic broken line to its diameter

$$F=4f. \tag{27}$$

The definition of θ is clearer from Fig. 4(b). Let us recall that the original Koch curve, Fig. 4(a), corresponds to $\theta=\sqrt{3}/2$. The member $K_{\theta,n}$ of the sequence $\{K_{\theta,n}\}$, i.e., the member that is the result of $(n-1)$-fold applications of the iteration, is the broken line with 4^{n-1} segments, the length of each segment $s(n)$ being equal to

$$s(n)=f^{n-1}, \tag{28}$$

whereas the total length of $K_{\theta,n}$ is

$$S(n)=F^{n-1}. \tag{29}$$

Owing to its construction, the curve K_θ is self-similar, so it is a fractal curve whose fractal dimension is equal to

$$D_{K_\theta}=\lim_{n\to\infty}[1+\log_{1/s(n)}S(n)]=1+\log_{1/s(n)}S(n)=1+\log_{1/f}F$$

$$=\frac{\ln(F/f)}{\ln(1/f)}=\frac{2\ln 2}{\ln 2+\ln(1+\sqrt{1-\theta^2})}. \tag{30}$$

Thus D_{K_θ} obeys the asymptotic relations

$$D_{K_\theta}\to\begin{cases}2-\dfrac{2}{\ln 2}\sqrt{1-\theta^2} & \text{for} \quad \theta\to 1\\[2ex] 1+\dfrac{1}{8\ln 2}\,\theta^2 & \text{for} \quad \theta\to 0.\end{cases} \tag{31}$$

The fractal excess $\Delta D_{K_\theta}\equiv D_{K_\theta}-1\to\theta^2/(8\ln 2)$ when $\theta\to 0$.

If a point A is a vertex of a broken line $K_{\theta,n}$, then $A\in K_\theta$. Let us consider two points A and $B\in K_\theta$ that are extreme points of the same segment of a broken line $K_{\theta,n}$ for some n. Any line $K_{\theta,n}$ may be treated as a smoothed version of the curve K_θ over spatial scales that are rigorously smaller than $s(n)$. Now let us take $m\geqslant 1$ and denote $l_{\min}\equiv s(n+m)$ for a curve $K_{\theta,n+m}$. Let $S_{l_{\min}}(AB)$ be a distance between A and B *along* the curve $K_{\theta,n+m}$. The shortest ''wavelength'' of ''disturbances'' corresponding to the curve $K_{\theta,n+m}$ is $l_{\min}=f^{n+m-1}$. If we define $l_{\max}\equiv|AB|=f^{n-1}$ to be the order of the longest wavelength of disturbances that can be placed between A and B, then we have

$$S_{l_{\min}}(AB)=|AB|\left(\frac{l_{\max}}{l_{\min}}\right)^{D_{K_\theta}-1}, \tag{32}$$

with D_{K_θ} being the same as in Eq. (30). By the way, one can give another derivation of Eq. (32) immediately if one keeps in mind the definition, generalizing Eq. (1) for an interval of a one-dimensional curve.

According to Eq. (31), $\Delta D_{K_\theta}\to 0$ when $\theta\to 0$. Hence, if

$$1\ll\frac{l_{\max}}{l_{\min}}\ll\exp\frac{1}{\Delta D_{K_\theta}}$$

for $\Delta D_{K_\theta}\to 0$, then

$$S_{l_{\min}}(AB)=|AB|\left(1+\Delta D\ln\frac{l_{\max}}{l_{\min}}+\cdots\right) \tag{33}$$

and the relative correction of $S_{l_{\min}}(AB)$ with respect to $|AB|$ is small.

Let us consider again some point A belonging to the curve K_θ and a circle centered at the point A with radius r, so that the circle intersects the curve K_θ at least at two points situated on opposite sides of the curve K_θ relative to A. Choose the points B and C nearest to A along K_θ and belonging to the opposite intersections mentioned above. It is interesting that owing to the construction of K_θ, the angle between vectors $\overrightarrow{AB}$ and $\overrightarrow{CA}$ is small for small θ and of order θ. This

important fact does not depend on the value of r and is true even for arbitrarily small r. It does not contradict, however, the statement that in any, even a very small, vicinity O_ε of each point $A \in K_\theta$, we can find a point $B \in O_\varepsilon \cap K_\theta$ such that the vector $\overrightarrow{AB}$ has an arbitrary direction.

These properties of the generalized Koch fractal curve can be expressed, when $\theta \to 0$ and $\Delta D \to 0$, by the following statements.

(a) The curve K_θ is very ''smooth'' on average in arbitrarily small scales, whereas it is not differentiable and not smooth locally.

(b) The distance along the smoothed curve K_θ between two points A and B belonging to the curve K_θ, which is smoothed over the scales less than $l_{\min}$, differs only slightly from the shortest distance $|AB|$ between these points while

$$l_{\min} \gg |AB| \exp(-1/\Delta D), \tag{34}$$

which is extremely small with respect to $|AB|$ when $\Delta D \to 0$; see Eq. (33).

(c) The curve K_θ smoothed over the scales that are less than $l_{\min}$ can be described by the equation

$$y = h(x) \quad \text{with} \quad |dh/dx| \ll 1 \tag{35}$$

in the proper Cartesian coordinates provided that $l_{\min}$ obeys the inequality (34).

We believe that the properties (a)–(c) are general properties of any ''normal'' fractal curve with small ΔD.

VI. ANALYTIC ESTIMATION OF THE FRACTAL EXCESS WITH THE AID OF THE SIVASHINSKY EQUATION

Comparing property (c) of the generalized Koch fractal curve with Eqs. (15)–(17), one sees that the Sivashinsky equation (17), as well as Eq. (20), may be a very useful model for the Frankel equation (15). For this reason it is interesting to consider properties of stochastic solutions of the Sivashinsky equation in some detail.

Consider a stochastic solution of Eq. (20) for arbitrarily large $t \to \infty$, if a very low noise is supposed as the initial condition at $t = 0$. Due to the intrinsic instability of Eq. (20), the strongly nonlinear regime of this instability should take place at the moment t in the following range of spatial scales l

$$1 \ll l \ll t, \tag{36}$$

whereas for $l \gg t$ the growth rate is too low for this instability to develop appreciably and for $l \ll 1$ strong damping of disturbances takes place due to the Markstein diffusion. The two-point correlation function of the Sivashinsky equation and its Fourier transform may be defined as

$$\langle \eta(x,t)\, \eta(x',t) \rangle = G(x - x', t), \tag{37}$$

$$\eta_k^2(t) \equiv \overline{G}(k,t) = \frac{1}{2\pi} \int G(x,t) e^{-ikx} dx, \tag{38}$$

where $\langle\ \rangle$ denotes a certain spatial averaging. The scaling (23) of Eq. (22) or solutions of Eq. (20) in the range (36) should lead to the invariance of the two-point correlation function in the relevant range of the wave vectors with respect to this scaling. Then

$$\eta_k^2(t) = \frac{d_0(2)}{2} \frac{1}{|k|^3} + \cdots \quad \text{for} \quad \frac{C_1}{t} \ll |k| \ll C_2. \tag{39}$$

Here $d_0(2)$, C_1, and C_2 are some unknown positive constants, as well as C_i (for $i = 3,4, \ldots$) entering the expressions below. They should be of the order of unity since Eq. (20) does not contain any large or small coefficients. The number 2 in $d_0(2)$ refers to the dimension of the ambient space in which the flame front propagates.

This important result can be obtained in a more physical manner (see Ref. [8]), which clarifies basic assumptions for Eq. (39) validity. Let $\overline{\eta}(k,t)$ be the Fourier transform of $\eta(x,t)$ and

$$\tilde{\eta}_k(x,t) = \int_k^{2k} \overline{\eta}(k,t) \exp(ikx)\, dk \tag{40}$$

be typical disturbances with the wavelengths of the order of $2\pi/k$ for $1/t \ll k \ll 1$. Then it is quite natural that for $\tilde{\eta}_k(x,t)$ all terms in Eq. (22) are on average equal to each other by the order of magnitude when $1/t \ll k \ll 1$. This natural assumption leads to Eq. (39). Notice that the right-hand side of Eq. (22) describes the linear instability, whereas the term $(\nabla \eta)^2/2$ corresponds, in distinction to all others, to a nonlinear attenuation. If the considered property is expressed in terms of $\tilde{h}$ instead of $\tilde{\eta}$, with $\tilde{h}$ being defined analogously to $\tilde{\eta}$ in Eq. (40), then it gives a relation

$$|\partial \tilde{h}_k / \partial x| \sim \gamma \tag{41}$$

for any k belonging to the range $1/\gamma t \ll k \ll \gamma$.

The latter consideration implies that an interaction of disturbances with a high value of their typical spatial scale ratios, which can be both direct and by means of a cascade, plays a minor role in the formation of the level of quasistationary fluctuations relative to interactions of modes with comparable wavelengths and to competition of the latter nonlinear process with the linear growth rate. Indeed, Eq. (21) shows only a trivial action of a longer wave on a considered one, whereas a shorter wave leads mainly to the front velocity renormalization, which is proportional to $\langle (\nabla \eta)^2 \rangle/2$ with averaging over the shorter wavelengths. Additional arguments illustrating the role of coherent cascade processes can be obtained by the analysis of exact ''laminar'' stationary solutions of Eq. (22) [29], which should be regularized by the term $\varepsilon \nabla^2 \eta$ (with $\varepsilon \to 0$). The existence of the cusps in these exact nonlinear solutions leads to a decrease of the noise spectral density at high k, which is steeper than suggested by Eq. (39). The contribution of cusps to the noise spectral density is proportional to $(kl)^{-4} \ln^2(kl)$ for $kl \gg 1$, where l is the distance between the cusps. The consideration of the Sivashinsky equation presented above suggests that the fluctuation level near a fixed wavelength is determined mainly by linear and nonlinear interactions with fluctuations whose wavelengths are of the order of a fixed one, but not by direct or indirect interactions with fluctuations whose wavelengths are much longer or shorter (of

course, the real dissipation of the fluctuation energy takes place in the region of $k \gtrsim 1$ only). Thus the Sivashinsky equation (20) differs qualitatively from the Kuramoto-Sivashinsky equation [37], for example, where the interaction of modes of very different spatial scales is very important.

Using the two-point correlation function (39), one can find other important properties of the stochastic solutions of the Sivashinsky equation:

$$\langle [\eta(x)-\eta(x')]^2 \rangle \approx d_0(2)(x-x')^2 \ln \frac{C_3 t}{|x-x'|}$$

$$\text{for } C_4 t \gg |x-x'| \gg C_5, \qquad (42)$$

$$\langle (\partial_x \eta)^2 \rangle \approx 2 d_0(2) \ln C_6 t \quad \text{for } t \gg C_7, \qquad (43)$$

where $\partial_x \equiv (\partial/\partial x)$. The integrals, needed to obtain Eqs. (42) and (43) from the Fourier transform of the two-point correlation function, diverge at upper and lower limits but only logarithmically, as soon as the asymptotic form (39) of the two-point correlation function is substituted. This allows us to evaluate them successfully with relative accuracy of the order of $1/\ln t$. The relationship (43) can be rewritten in the form

$$\langle (\partial_x \eta)^2 \rangle \approx 2 d_0(2) \ln(l_{\max}/l_{\min}) \qquad (44)$$

with the same accuracy if the typical maximum and minimum wavelengths of disturbances are denoted by $l_{\max}$ and $l_{\min}$, respectively, with $l_{\max} \sim t$ and $l_{\min} \sim 1$.

Turning now to the unscaled form (17) of the Sivashinsky equation and taking into account the proper rescaling, we notice that the value of $\langle (\partial_x h)^2 \rangle/2$ gives the following correction to the mean front velocity:

$$\delta u \equiv u - u_0 = \langle (\partial_x h)^2 \rangle u_0/2 = u_0 d_0(2) \gamma^2 \ln(l_{\max}/l_{\min}), \qquad (45)$$

where $u_0 \equiv 1$ in our units, whereas the correction to the front ''length'' between points x and x' is

$$S(x,x') - |x-x'| \approx |x-x'| \langle (\partial_x h)^2 \rangle/2 \approx |x-x'| d_0(2) \gamma^2 \ln(l_{\max}/l_{\min}). \qquad (46)$$

It appears from the viewpoint of the definition (3) that the fractal excess corresponding to the Sivashinsky equation is exactly equal to zero. This statement contradicts the opinion expressed in Ref. [23], where the value of $\Delta D = 0.3$ is claimed. But more attentive examination of the last paragraph of Sec. 4 in Ref. [23] and of the accompanying Table 1 therein reveals that, for small scales, $\ln l \leqslant 7.6$ in our notation, where the fractal excess *must* be determined, the value of $\Delta D = 0.01$ is actually found numerically in [23]. Given numerical noise, this does not contradict our result $\Delta D = 0$ implied by Eq. (46).

Comparing now Eq. (46) with Eq. (33), the following important statement can be formulated. The fractal excess of the flame front surface (which is actually a curve here) governed by the Frankel equation can be expressed in terms of the coefficient $d_0(2)$ in the asymptotic two-point correlation function; see Eq. (39):

$$\Delta D = d_0(2) \gamma^2 \quad \text{for } \gamma \to 0. \qquad (47)$$

This almost obvious statement, if we keep in mind Eqs. (33), (35), (15)–(17), and (46), is, however, in need of additional arguments.

Let us consider a curve $\Sigma(t)$ governed by the Frankel equation (14) for time $t \to \infty$ in the case when $\gamma \to 0$, but

$$\frac{\lambda_{\max}}{\lambda_{\min}} \sim \gamma^2 t \gg \exp \frac{1}{\Delta D(\gamma)}. \qquad (48)$$

Let us also divide the whole range of typical wavelengths of the front bends $(\lambda_{\min}, \lambda_{\max})$ in N subranges (l_{i-1}, l_i) with $i = 1,2,\ldots,N$, so that $l_0 = \lambda_{\min}$, $l_N = \lambda_{\max}$, and

$$1 \ll \frac{l_i}{l_{i-1}} = Q \ll \min\left\{ \exp \frac{1}{d_0(2)\gamma^2}, \exp \frac{1}{\Delta D(\gamma)} \right\}, \qquad (49)$$

with Q independent of the number i. For example, $Q \sim \min\{\exp[1/\gamma\sqrt{d_0(2)}],\ \exp[1/\sqrt{\Delta D(\gamma)}]\}$ and N being equal to the integer part of $\ln(\lambda_{\max}/\lambda_{\min}) \max\{\gamma\sqrt{d_0(2)}, \sqrt{\Delta D(\gamma)}\}$ can be admitted as a suitable example. For each interval (l_{i-1}, l_i), consider a curve Σ_i, which is the result of a smoothing of the curve Σ over scales which are less than l_{i-1}. If Q is sufficiently high, then the influence of shorter wavelengths can be taken into account by introducing a new renormalized seed velocity u_{i-1} of the curve Σ_i, which is laminar from the viewpoint of the longer wavelengths. Let us also divide the curve Σ_i in curved intervals of the length l_i. Each of these intervals of Σ_i can be described with high accuracy by the Sivashinsky equation (17) (where the last term in the right-hand side may be kept only as a regularizing factor) in the proper Cartesian coordinate systems, with Eqs. (15) and (16) being valid automatically owing to our choice of the set $\{l_i\}_{i=1,\ldots,N}$; see the second argument of min(,) in relation (49). For these coordinate systems, the angle of rotation with respect to each other may be arbitrarily large if the distance between relevant intervals is sufficiently large. So the reason why the Sivashinsky equation is not an exact model of the Frankel equation lies in their different properties with respect to rotational symmetry of the problem. Thus

$$h_k^2 \approx \frac{d_0(2)}{2} \gamma^2 \frac{1}{|k|^3} \quad \text{for } \frac{2\pi}{l_i} \ll k \ll \frac{2\pi}{l_{i-1}}, \qquad (50)$$

in accordance with Eq. (39), and the renormalized laminar front velocity u_i for Σ_{i+1} can be expressed through the renormalized laminar front velocity u_{i-1} of Σ_i, taking into account the front bends with typical curvature radius being between l_{i-1} and l_i in the manner

$$u_{i+1} = u_i \left(1 + d_0(2) \gamma^2 \ln \frac{l_i}{l_{i+1}} \right) = u_i [1 + d_0(2) \gamma^2 \ln Q]. \qquad (51)$$

This equation is a perfect analogy of Eq. (45). Collecting iteratively all corrections to velocities of the fronts Σ_i, we obtain for the front velocity

$$u \equiv u_N = \frac{u_N}{u_{N-1}} \frac{u_{N-1}}{u_{N-2}} \cdots \frac{u_1}{u_0} u_0 = u_0 [1 + d_0(2)\gamma^2 \ln Q]^N$$

$$= u_0 \exp[d_0(2)\gamma^2 N \ln Q] = u_0 (Q^N)^{d_0(2)\gamma^2} = u_0 \left(\frac{\lambda_{\max}}{\lambda_{\min}} \right)^{\Delta D}, \tag{52}$$

where ΔD is determined by Eq. (47) and the fourth equality is valid because $d_0(2)\gamma^2 \ln Q \ll 1$ owing to our construction. This consideration does not take into account exactly the scales that are comparable to l_i, $i = 1,2, \ldots, N$. However, even $\ln(l_{i+1}/l_i)$ is very high for $\gamma \to 0$, so this inaccuracy leads to an error in our expression for ΔD only of the order of γ^3 for $\gamma \to 0$.

We have completed now the derivation of the relationship between the fractal excess of the Frankel equation solutions and the properties of the two-point correlation function of the corresponding Sivashinsky equation. It may be noted here that the property (41) of the stochastic solutions of the Frankel equation corresponds obviously to the construction of the generalized Koch curve in Sec. V, so that θ can be compared with γ by the order of magnitude, when θ and $\gamma \to 0$. From this point of view, a certain analogy between Eqs. (31) and (47) is no wonder. The proposal of Eq. (8) was used in Ref. [8] and that is why we consider the generalized Koch construction in some detail. This illustration is needed to show the development of large angles between normals to the perturbed and unperturbed fronts even for a very small γ. There are two properties of the generalized Koch curve (with a small height of its basic element) that make it important for the flame problem: (i) its basic element is similar to a saturated LD wave near the minimum nonlinearly unstable wavelength and (ii) the ratio of the amplitude of the saturated ''plane'' LD wave to its length is the same on all larger scales, similar to the Koch curve. This analogy helps us to understand that there is no paradox in applying nonfractal Sivashinsky equation to fractal flames. As discussed in this section, we apply the Sivashinsky equation only to a smoothed flame with renormalized speed and in a proper Cartesian system where there are no large angles and no fractal behavior because of the smoothing.

The main results of this section can be summarized as follows.

(i) The fractal excess of the flame front governed by the Frankel equation is proportional to γ^2; see Eq. (8).

(ii) The coefficient in Eq. (8) can be expressed in terms of the asymptotic form of the two-point correlation function of the Sivashinsky equation

$$D_0 = d_0(2), \tag{53}$$

though the fractal excess for the Sivashinsky equation itself is equal to zero.

VII. FURTHER SIMULATIONS AND ESTIMATION OF D_0

We have no opportunities to find $d_0(2)$ in Eq. (39) analytically, in order to determine D_0 with the help of Eq. (53). Moreover, some considerations in Secs. II and VI cannot be considered as rigorous proofs from a mathematical point of view. For these reasons the simulation of the Frankel equation is highly desirable to check the functional form of Eq. (8) and to evaluate the constant D_0. To do this for low γ we need to continue our runs for a much longer time than is reasonable with the full quasicircular mesh used to produce Figs. 2 and 3. We have developed a special version of our code that allows us to follow the evolution of flames up to times of a few thousand (in Markstein units).

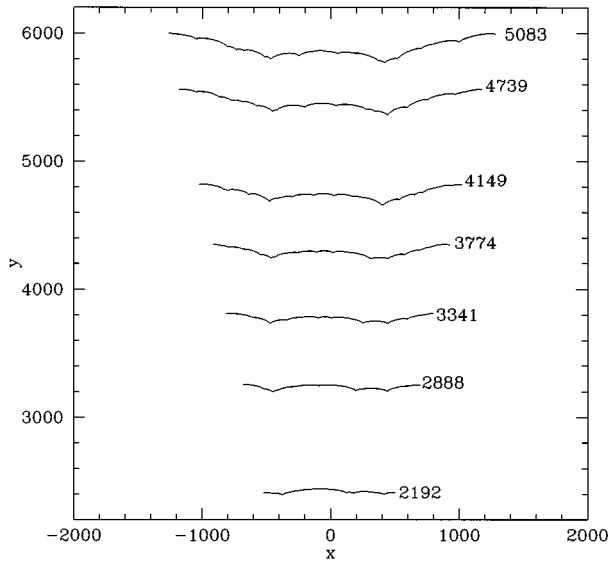

FIG. 5. Part of the whole front ''circle'' for $\gamma = 0.35$ at different moments of time t labeling the curves. This picture should be imagined to be continued periodically onto the whole circle to obtain the pattern of the whole front whose center is at $x = 0$, $y = 0$.

Our simulations of the Frankel equation for $\gamma = 0.3$, 0.35, and 0.4 with this version of the code are presented here. To keep the used CPU time of the Cray Y-MP supercomputer in the limits of a few hours even for $\gamma = 0.3$ under the condition that the front develops for a sufficiently long time in a saturated nonlinear regime of the LD instability, we simulate only a part of a whole ''circle'' of the front, continuing the solution periodically onto the whole circle. It is justified because the disturbances with sufficiently low azimuthal wave numbers m do not grow in accordance with the linear theory of the LD instability for low γ due to the stretching effect [3,30]. (See also Fig. 3.) The sector, where the flame propagation is actually simulated, is $2\pi/m_0$, with $m_0 = 18,15,13$ for $\gamma = 0.3, 0.35, 0.4$, respectively. The initial radius r_0 is perturbed according to the expression

$$\delta r / r_0 = 0.05\gamma^2 \sum_{n=1}^{12} 2^{-n} \cos(2^n m_0 \varphi - 2\pi r_n), \tag{54}$$

where φ is the azimuthal angle, $r_n \in [0,1]$ is a random number, and $r_0 \approx 500 - 750$ for $\gamma = 0.4 - 0.3$. The front patterns at different moments of time for $\gamma = 0.35$ in these series of our simulations are shown in Fig. 5 as an example.

The main goal of this simulation series is to determine the dependence of the fractal excess ΔD on the expansion degree γ. The relevant results are displayed in Fig. 6 and in Table I. Though the best power fit to these results is $\Delta D = 0.53\gamma^{2.6}$, the square dependence of ΔD on γ [see Eq. (47)] and the approximation (8) with

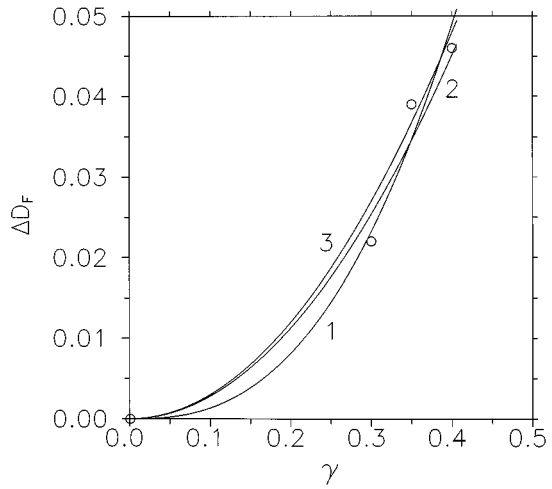

FIG. 6. Fractal excess (ΔD) dependence on the expansion degree (γ) obtained from our simulations of the Frankel equation (open circles) and different numbered fits (solid lines). Line 1 corresponds to the best power fit ($\Delta D = 0.53\gamma^{2.6}$), 2 to the best-squares fit ($\Delta D = 0.28\gamma^2$), and 3 to Eq. (8) with $D_0 = 0.3$.

$$D_0 = d_0(2) \approx 0.3 \tag{55}$$

do not contradict them, taking into account possible inaccuracies of simulations, whereas the best-squares fit is $\Delta D = 0.28\gamma^2$. We think that the accuracy of our estimation of D_0 is not too high and may be estimated as 50%. For this reason it is worth submitting here our procedure of calculation of D based on the results of the Frankel equation simulations.

Using the mesh point coordinates x_i, y_i we define

$$s_i = [(x_i - x_{i-1})^2 + (y_i - y_{i-1})^2]^{1/2} \tag{56}$$

for $i = 2,3,\ldots,N$ and calculate the total length of the front sector used in simulations, $s(t_m) = \Sigma_{i=2}^{N} s_i$, for a discrete set of time moments $\{t_m\}$ covering the whole time interval of simulation. For the same set $\{t_m\}$ we save the values of the mean radius $\overline{r}(t_m)$, defined by the relation

$$\overline{r^2} = \sum_{i=1}^{N} (x_i^2 + y_i^2)/N. \tag{57}$$

Then we find the least-squares linear fit to the relation $\ln s(t_m) - \ln \overline{r}(t_m)$ and the slope of the fit gives us the value of D actually used in our results presented in Fig. 6 and in Table I.

Another way to estimate D is to form (for a given moment t_p) an array of mean lengths of the front segments between the mesh points with numbers differing by j:

$$d_s(j) = \frac{2}{N} \sum_{i=1}^{N/2} \sum_{k=i+1}^{i+j} s_k \tag{58}$$

for $j = 1,2,\ldots,N/2$. One can also form an array of mean distances of the same pairs of points:

$$d_r(j) = \frac{2}{N} \sum_{i=1}^{N/2} [(x_i - x_{i+j})^2 + (y_i - y_{i+j})^2]^{1/2}. \tag{59}$$

Now the mean slope of the relation $\ln d_s(j) - \ln d_r(j)$ would give another estimate of the fractal dimension. This estimate can be done for only a few moments of time t_p when we save the data for all mesh points, contrary to the estimate based on the $\ln s(t_m) - \ln \overline{r}(t_m)$ relation, which is based on averaging over many thousands of moments t_m. Moreover, the procedure described by Eqs. (58) and (59) tends to underestimate the value of the fractal excess ΔD.

It is worth discussing here two important items of the Frankel equation simulation technique. The first one is a problem of self-intersections and the second one is the main source of the uncertainties of ΔD calculation.

It can be seen from our results that a typical pattern of the front curve just before a self-intersection can be sketched by the left-hand side of Fig. 1. See also a ''real'' example in Fig. 2. A self-intersection arises when one or even more ''elementary'' disturbances having the shape of an arc, being convex toward the direction of the front propagation, are near the vertex of a deep cusp. Let us approximate the shape of the cusps by exact solutions [29] of the Sivashinsky equation. They are valid for our purpose at sufficient distance from the cusp, where the front slope relative to the reference straight line is small with respect to unity. In the region whose distance from the cusp vertex is at the same time much less than the typical distance l_c between the deepest cusps, the front shape can be expressed, in accordance with the exact solutions [29], as

$$y = F(x - x_c) = \gamma |x - x_c| \ln \frac{l_c}{2|x - x_c|}. \tag{60}$$

A typical length of the shortest elementary disturbances, which is $|CD|$ in Fig. 1, is of the order of $30/\gamma$; see Sec. IV. A self-intersection can really take place only when the slope of the front to the reference line is at least of the order of

TABLE I. Simulated fractal dimension D of the front surface governed by the Frankel equation (14) as a function of the expansion degree γ.

γ	D	Best power fit[a]	Best-squares fit[b]	Eq.(8)[c]
0.3	1.022	1.023	1.025	1.027
0.35	1.039	1.036	1.034	1.037
0.4	1.046	1.049	1.045	1.048

[a] $\Delta D = 0.53\gamma^{2.6}$.
[b] $\Delta D = 0.28\gamma^2$.
[c] With $D_0 = 0.3$.

unity or even more at the distance of $|CD|\sim 30/\gamma$ from a deep cusp. This condition corresponds to the inequality

$$\ln\frac{\gamma^2 R}{60}\gtrsim\frac{1}{\gamma}, \tag{61}$$

where l_c is replaced by the maximum unstable wavelength and R is the mean radius of the front. This condition for the R available, i.e., for the physical time available in our simulations, can be fulfilled only when $\gamma\gtrsim 0.5$. This agrees with the fact of the absence of self-intersections in our simulations when $\gamma<0.5$. Almost the same consideration allows us to estimate the longest perimeter H_u of the detached drops of unburned matter

$$H_u\sim l_c\exp(-1/\gamma). \tag{62}$$

Thus the contribution of the lengths of the detached drops perimeter, which appear due to self-intersections, decreases proportionally as $\exp(-1/\gamma)$, i.e., faster than any power of γ, when $\gamma\to 0$. Taking into account our main result (8), it can be seen that self-intersections play only a minor role in the front acceleration when $\gamma\ll 1$.

The same peculiarities [see Eq. (60)] of the cusp shape lead, however, to other difficulties of the Frankel equation simulations. Only comparatively small regions near the cusps, whose length is only about 1/10 of the distance between the cusps of considered depth, are responsible for the main contribution to the front length correction in the Sivashinsky approximation. In our simulations (given the number of mesh points, CPU time, etc.) this distance is comparable to the shortest unstable wavelength, for which the Markstein diffusivity plays a noticeable role in contrast to long-wavelength disturbances, when $\lambda_{\max}/\lambda_{\min}\to\infty$. Then the accuracy of the self-similarity of the front curve is rather low. As a result, different methods of the fractal excess calculations, which are equal to each other when $\lambda_{\max}/\lambda_{\min}\to\infty$, give somewhat different results. It was easily detected by us and determines actually the accuracy of D_0 quoted above.

VIII. THE FRONT SURFACE IN THREE-DIMENSIONAL SPACE

In the foregoing we considered only the two-dimensional case, when the front corresponds to a curve in two-dimensional space. Almost all results (with the obvious exception of the results of simulations) can be generalized on the three-dimensional case, when the front is represented as a surface, which is denoted in this section again as Σ. We introduce here the main equations in the three-dimensional case without repeating detailed explanations.

Equation (11) should be replaced by

$$U(\vec{x},t)=\frac{J(\vec{x},t)}{\rho_b}-\frac{\gamma}{2\rho_b}\left(J(\vec{x},t)-\frac{1}{2\pi}\int_{\Sigma(t)}J(\vec{\xi},t)\frac{(\vec{x}-\vec{\xi})\cdot\vec{n}(\vec{x},t)}{|\vec{x}-\vec{\xi}|^3}d\Sigma_\xi\right), \tag{63}$$

where $d\Sigma_\xi$ is a differential of area of Σ. Equation (13) keeps its form with the old definition of $\mathscr{K}$: $\mathscr{K}=(\operatorname{div}\vec{n})|_{\vec{x}\in\Sigma}$, so $\mathscr{K}$ is now the sum of the principal values of the surface curvature. Equation (14) should be replaced by

$$U(\vec{x},t)=1-\operatorname{div}\vec{n}(\vec{x},t)-\frac{\gamma}{2}\left(1-\frac{1}{2\pi}\int_{\Sigma(t)}\frac{(\vec{x}-\vec{\xi})\cdot\vec{n}(\vec{x},t)}{|\vec{x}-\vec{\xi}|^3}d\Sigma_\xi\right). \tag{64}$$

In the Sivashinsky equations of different forms [Eqs. (18), (20), and (22)], the functions $h(x,t)$, $\eta(x,t)$, and the operator $\partial/\partial x$ should be replaced obviously by $h(x,y,t)$, $\eta(x,y,t)$, and the nabla operator ∇ [in (x,y) space], respectively, and the factor $1/(4\pi)$ in the definition of $I\{\}$, Eq. (18), should be replaced by $1/(8\pi^2)$. Thus Eq. (20) has the following form in the three-dimensional case:

$$\frac{\partial\eta}{\partial t}+\frac{1}{2}(\nabla\eta)^2=I\{\eta\}+\nabla^2\eta. \tag{65}$$

The main results of Sec. VI do not depend seriously on the space dimension. The Fourier transform of the two-point correlation function $G(\vec{w})\equiv\langle\eta(\vec{x})\,\eta(\vec{x}+\vec{w})\rangle$ should have in the similarity range the asymptotic form

$$\eta^2_{\vec{k},t}=\frac{d_0(3)}{2\pi}\frac{1}{k^4}+\cdots\quad\text{for}\quad\frac{C_8}{t}\ll k\ll C_9, \tag{66}$$

where $d_0(3)$ is again an unknown positive constant. As a result, Eqs. (42), (43), and (44) should be replaced by

$$\langle[\eta(\vec{x})-\eta(\vec{x}')]^2\rangle\approx\frac{1}{2}d_0(3)(\vec{x}-\vec{x}')^2\ln\frac{C_{10}t}{|\vec{x}-\vec{x}'|}\quad\text{for}\quad C_{11}t\gg|\vec{x}-\vec{x}'|\gg C_{12}, \tag{67}$$

$$\langle(\nabla\eta)^2\rangle\approx 2d_0(3)\ln C_{13}t, \tag{68}$$

and

$$\langle(\nabla\eta)^2\rangle\approx 2d_0(3)\ln\frac{l_{\max}}{l_{\min}}, \tag{69}$$

respectively. Thus, for the fractal dimension of a front governed by the Frankel equation we can write $\Delta D=d_0(3)\gamma^2$, when $\gamma\to 0$.

The Sivashinsky equation (65) governing the front surface in the three-dimensional space has the following interesting property quoted in Ref. [30]. If $\eta=f_1(x,t)$ and $\eta=f_2(x,t)$ are arbitrary general solutions of Eq. (20), then

$$\eta(x,y,t)=f_1(x,t)+f_2(y,t) \tag{70}$$

is a solution (but only a particular one) of Eq. (65). Inserting this particular solution in Eqs. (68) and (69), we find that they keep their validity [because of Eqs. (45) and (46)] after substituting $2d_0(2)$ instead of $d_0(3)$. Assuming that statisti-

cal properties of the solution (70) can approximate, to a certain degree, the properties of a general solution, we can write $d_0(3) \approx 2d_0(2)$ with the same degree of accuracy. Hence the fractal dimension of the front surface governed by Eq. (64) can be approximated as the double fractal dimension of the front curve governed by Eq. (14), when $\gamma \to 0$.

IX. DISCUSSION

The main result of this work is that the flame front wrinkled by the Landau-Darrieus instability can be approximated in a certain range of spatial scales by a fractal surface whose fractal dimension excess tends to zero in accordance with Eq. (8), when the expansion degree γ tends to zero. More complete general conclusions are quoted in the Introduction and the coefficient of the asymptotic relation (8) is considered in Sec. VII.

The results of our numerical simulations agree well with the main qualitative conclusion of [23]: we observe, as they do, the phenomenon of cell splitting, which is observed also experimentally for expanding flames [11]. One should remember that in Ref. [23] a version of the front equation is used that is not strictly equivalent to the original Sivashinsky equation (17): Filyand *et al.* [23] modify the equation in order to include the effects of sphericity of an expanding flame. We have presented arguments showing that the fractal excess of wrinkled flames modeled with the Sivashinsky equation (17) is zero. As we have noted, this does not contradict the results of [23] for small segments of their simulated flame, where Eq. (17) is applicable.

An interesting question arises when we compare our results with those of Joulin [30]. He derived rigorously a modification of the Sivashinsky equation for spherical flames (structurally equivalent to that used in [23]) but, contrary to [23] and to our simulations of the Frankel equation, he found (using the pole decomposition method as in [29]) that there was no tendency to repeated cell splitting. The Frankel equation is not equivalent to the equations used in [23,30], but one cannot exclude that the effect of cell splitting found here and in [23] is produced by numerical noise. Besides ever-present rounding and truncation errors, the spectral method used in [23] generates noise whenever the number of the Fourier harmonics is changed, whereas our technique produces perturbations when we remove or insert mesh points. Since perturbations of a very small (''exponentially'' small) amplitude are detected and amplified by the Landau instability, it is no wonder that new corrugations appear repeatedly in numerical modeling. A less trivial task is to find out if this spontaneous tendency is closer to real flames than a much more laminar behavior predicted by semianalytic solutions [30].

Joulin [30] writes about the external noise for real (not numerical) flames: ''It is difficult to imagine why this noise should be compatible with large-scale, angular periodicity corresponding to an $O(1)$, but otherwise arbitrary, sector; instead a fixed, small-scale, average spatial size is expected, especially if the noise has a hydrodynamic origin.'' We cannot agree that the latter statement is always true: the hydrodynamic noise must not be necessarily of the external origin.

One should not forget that the vorticity arises on the wrinkled front, which is neglected in the Frankel (and Sivashinsky) approach. As a result, a region of a complicated vortical turbulent motion may always exist far enough behind the front. A turbulent cascade of vortices can generate the noise needed, so the flame may well be self-organized with scales dictated by the LD instability.

There is another consequence of the vortex generation. A magnitude of the generated vorticity increases in accordance with Eq. (10), when the expansion degree γ grows. So a region of a complicated vortical turbulent motion extends in the upstream direction and can absorb the flame front when γ exceeds some critical value. This can be examined with the aid of results of the two-dimensional numerical simulations performed by Niemeyer and Hillebrandt (see Ref. [9]). They simulated full hydrodynamics of the burning front propagation as well as processes of burning itself and heat transport (but using out of necessity a rather small physical size of a simulated region). For small γ (when $\gamma \lesssim 0.3$), the front shape obtained in Ref. [9] is quite similar to that obtained here. However, our investigation corresponds to a significantly wider range of spatial scales owing to the use of the Frankel equation, which allows us to evaluate the fractal characteristics of the flame.

From the results of Ref. [9] it may be concluded that for $\gamma \gtrsim 0.5$ the gas motion in the vicinity of the front becomes turbulent. If this turbulence acts on the flame front similarly to the external turbulence, then the fractal dimension of the flame should be equal to 7/3 in three-dimensional space (see Ref. [14]), when $\gamma \gtrsim 0.5$. The value 7/3 seems to be in accordance with the experimental results reviewed in Ref. [11].

However, it is not clear at present what the primary reason for growing turbulence observed in Ref. [9] for $\gamma \simeq 0.5$ is. It could be just the tendency of front to self-intersection, which we find exactly for $\gamma \gtrsim 0.5$. If so, then the vorticity plays only a secondary role, since it is completely ignored in our numerical experiments and analytical estimates. The estimates presented in Ref. [38] do show that vortical self-turbulence is rather mild. It would be very interesting to investigate this question in more detail, relaxing the approximation of potential flow, which is suspicious for $\gamma \gtrsim 0.5$.

ACKNOWLEDGMENTS

We are grateful to M. Basko, W. Hillebrandt, B. Meerson, J. Niemeyer, G.I. Sivashinsky, and S.E. Woosley for valuable discussions and for providing us with information on their results prior to publication. N. Ardelyan, O. Bartunov, and E. Müller gave us very useful help and advice on our numerical work. Part of the work was done during S.B.'s visits to University of California, Santa Cruz, and to Max Planck Institut für Astrophysik, Garching, and he is grateful to S.E. Woosley and to W. Hillebrandt for their hospitality. Max Planck Institute allocated Cray Y-MP computer time. This work is supported in part by the Russian Foundation for Fundamental Research (Grant Nos. 93-02-17114 and 94-01-01649) and by International Science (Soros) Foundation. The work of S.B. is supported by the National Science Foundation (Grant No. AST-91-15367) and by NASA (Contract No. NAGW-2525).

[1] L. D. Landau and E. M. Lifshitz, *Fluid Mechanics* (Pergamon, Oxford, 1959).
[2] L. D. Landau, Acta Physicochim. USSR **19**, 77 (1944) (see also a reprinted version in Ref. [4]).
[3] Ya. B. Zeldovich, G. I. Barenblatt, V. B. Librovich, and G. M. Makhviladze, *The Mathematical Theory of Combustion and Explosions* (Consultants Bureau, New York, 1985).
[4] P. Pelcé, *Dynamics of Curved Fronts* (Academic, Boston, 1988).
[5] A. Liñán and F. A. Williams, *Fundamental Aspects of Combustion* (Oxford University Press, New York, 1993).
[6] D. L. Frost, Phys. Fluids **31**, 2554 (1988).
[7] I. Aranson, B. Meerson, and P. Sasorov, Phys. Rev. E **52**, 948 (1995).
[8] S. I. Blinnikov, P. V. Sasorov, and S. E. Woosley, in *Proceedings of the Jubilee Gamow Seminar, St. Petersburg, 1994,* edited by A. Bykov and R. Chevalier (Kluwer Academic Publishers Space Science Reviews, Dordrecht, 1995), Vol. 74, p. 299.
[9] J. C. Niemeyer and W. Hillebrandt, Astrophys. J. **452**, 779 (1995).
[10] F. C. Gouldin, Combust. Flame **68**, 249 (1987).
[11] Y. A. Gostintsev, A. G. Istratov, and Yu. V. Shulenin, Fiz. Goreniya Vzryva **24**, 63 (1988) [Combust. Expl. Shock Waves **24**, 563 (1988)].
[12] S. E. Woosley, in *Supernovae*, edited by A. G. Petschek (Springer-Verlag, New York, 1990), p. 182.
[13] K. R. Sreenivasan, Annu. Rev. Fluid Mech. **23**, 539 (1991).
[14] P. Clavin, Annu. Rev. Fluid Mech. **26**, 321 (1994).
[15] F. X. Timmes and S. E. Woosley, Astrophys. J. **396**, 649 (1992).
[16] G. H. Markstein, J. Aeronaut. Sci. **18**, 199 (1951) (see also a reprinted version in Ref. [4]).
[17] P. Pelcé and P. Clavin, J. Fluid Mech. **124**, 219 (1982).
[18] M. Matalon and B. J. Matkovsky, J. Fluid Mech. **124**, 239 (1982).
[19] M. A. Liberman, V. V. Bychkov, and S. M. Goldberg, Zh. Éksp. Teor. Fiz. **104**, 2685 (1993) [Sov. Phys. JETP **77**, 227 (1993)].
[20] M. L. Frankel, Phys. Fluid A **2**, 1879 (1990).
[21] G. I. Sivashinsky, Acta Astronaut. **4**, 1177 (1977).
[22] G. I. Sivashinsky, Annu. Rev. Fluid Mech. **15**, 179 (1983).
[23] L. Filyand, G. I. Sivashinsky, and M. L. Frankel, Physica D **72**, 110 (1994).
[24] The latter restriction is necessary because we have used the linear theory of the LD instability, which supposes an infinitesimally thin front. The finite front thickness leads to an additional correction to $\vec{v}_v$ (see Ref. [18]), which, however, is much less than the estimation (10) whenever $\lambda \gg l_D$.
[25] S. Zhdanov and B. Trubnikov, Zh. Éksp. Teor. Fiz. **95**, 114 (1989) [Sov. Phys. JETP **68**, 65 (1989)].
[26] D. M. Michelson and G. I. Sivashinsky, Acta Astronaut. **4**, 1207 (1977).
[27] A. Pumir, Phys. Rev. A **31**, 543 (1985).
[28] Y. C. Lee and H. H. Chen, Phys. Scr. **T2**, 41 (1982).
[29] O. Thual, U. Frish, and M. Henon, J. Phys. (Paris) **46**, 1485 (1985).
[30] G. Joulin, Phys. Rev. E **50**, 2030 (1994).
[31] C. W. Gear, *Numerical Initial Value Problems in Ordinary Differential Equations* (Prentice-Hall, Englewood Cliffs, NJ, 1971).
[32] R. K. Brayton, F. G. Gustavson, and G. D. Hachtel, Proc. IEEE **60**, 98 (1972).
[33] J. Barnes and P. Hut, Nature **324**, 446 (1986).
[34] L. Hernquist, J. Comput. Phys. **87**, 137 (1990).
[35] J. Makino, J. Comput. Phys. **87**, 148 (1990).
[36] H. Gould and J. Tobochnik, *An Introduction to Computer Simulation Methods* (Addison-Wesley, Reading, MA, 1988).
[37] I. Procaccia, M. Jensen, V. S. L'vov, K. Sneppen, and R. Zeitak, Phys. Rev. A **46**, 3220 (1992).
[38] V. R. Kuznetsov and V. A. Sabel'nikov, *Turbulentnost' i Gorenie* (Nauka, Moscow, 1986) [*Turbulence and Combustion,* edited by P. A. Libby (Hemisphere, New York, 1990)].